THE JOURNAL OF BIOLOGICAL CHEMISTRY VOL. 291, NO. 20, pp. 10501–10514, May 13, 2016
© 2016 by The American Society for Biochemistry and Molecular Biology, Inc. Published in the U.S.A.

Mfsd2a Is a Transporter for the Essential ω-3 Fatty Acid Docosahexaenoic Acid (DHA) in Eye and Is Important for Photoreceptor Cell Development*

Received for publication, February 11, 2016, and in revised form, March 21, 2016 Published, JBC Papers in Press, March 22, 2016, DOI 10.1074/jbc.M116.721340

Bernice H. Wong[‡], Jia Pei Chan[‡], Amaury Cazenave-Gassiot[§], Rebecca W. Poh[¶], Juat Chin Foo[§], Dwight L. A. Galam[‡], Sujoy Ghosh[‡‖], Long N. Nguyen[**], Veluchamy A. Barathi[‡‡§§¶¶], Sia W. Yeo[‡‡], Chi D. Luu[‡‡‖‖], Markus R. Wenk[§], and David L. Silver[‡1]

From the [‡]Signature Research Program in Cardiovascular and Metabolic Disorders, [‖]Centre for Computational Biology, and [¶¶]ACP Ophthalmology, Duke-National University of Singapore Graduate Medical School, 8 College Road, Singapore 169857, Singapore, the [§]Department of Biochemistry, National University of Singapore, 8 Medical Drive, Block MD 7, Singapore 117597, Singapore, the [¶]Carl Zeiss Pte. Ltd., Microscopy Business Group, Singapore, 50 Kaki Bukit Place, 05-01, Singapore 415926, Singapore, the [**]Department of Biochemistry, Yong Loo Lin School of Medicine, National University of Singapore, 5 Science Drive 2, Building MD4, Level 1-03A, Singapore 117545, Singapore the [‡‡]Singapore Eye Research Institute, 11 Third Hospital Ave., Singapore 168751, Singapore, the [§§]Yong Loo Lin School of Medicine, National University of Singapore, 1E Kent Ridge Rd 119228, NUHS Tower Block, Level 11, Singapore 117597, Singapore, and the [‖‖]Centre for Eye Research Australia, Level 1, 32 Gisborne St., East Melbourne, Victoria 3002, Australia

Eye photoreceptor membrane discs in outer rod segments are highly enriched in the visual pigment rhodopsin and the ω-3 fatty acid docosahexaenoic acid (DHA). The eye acquires DHA from blood, but transporters for DHA uptake across the blood-retinal barrier or retinal pigment epithelium have not been identified. Mfsd2a is a newly described sodium-dependent lysophosphatidylcholine (LPC) symporter expressed at the blood-brain barrier that transports LPCs containing DHA and other long-chain fatty acids. LPC transport via Mfsd2a has been shown to be necessary for human brain growth. Here we demonstrate that Mfsd2a is highly expressed in retinal pigment epithelium in embryonic eye, before the development of photoreceptors, and is the primary site of Mfsd2a expression in the eye. Eyes from whole body Mfsd2a-deficient (KO) mice, but not endothelium-specific Mfsd2a-deficient mice, were DHA-deficient and had significantly reduced LPC/DHA transport *in vivo*. Fluorescein angiography indicated normal blood-retinal barrier function. Histological and electron microscopic analysis indicated that Mfsd2a KO mice exhibited a specific reduction in outer rod segment length, disorganized outer rod segment discs, and mislocalization of and reduction in rhodopsin early in postnatal development without loss of photoreceptors. Minor photoreceptor cell loss occurred in adult Mfsd2a KO mice, but electroretinography indicated visual function was normal. The developing eyes of Mfsd2a KO mice had activated microglia and up-regulation of lipogenic and cholesterogenic genes, likely adaptations to loss of LPC transport. These findings identify LPC transport via Mfsd2a as an important pathway for DHA uptake in eye and for development of photoreceptor membrane discs.

Docosahexaenoic acid (DHA)[2] is a conditionally essential ω-3 fatty acid highly enriched in neuronal tissues such as the brain and eye and is considered to be required for normal development and function of these tissues (1, 2), but the function of DHA in the retina is not understood. Within the eye, DHA is primarily found in phospholipids of photoreceptor outer segment (OS) membrane discs localized together with the photoreceptor rhodopsin (3) accounting for the highest body concentration of DHA per unit area (1). Like in brain, the eye does not synthesize DHA *de novo*, but must import it from the blood (1).

The eye contains two cellular barriers that prevent the diffusion of blood-borne material from entering the retina, the blood-retinal barrier (BRB) formed by the endothelium of retinal capillaries and the retinal pigment epithelium (RPE) at the back of the eye (4). DHA must cross these barriers for ultimate delivery to photoreceptor discs, but the contribution of either of these routes, via the BRB or RPE, to DHA uptake in the eye is unclear. Photoreceptors in OS discs exposed to daylight accumulate photo-damaged proteins and lipids over time (5). To cope with photo-damaged discs, photoreceptor outer segment discs undergo a constant renewal process for the maintenance of its excitability (6, 7). The RPE plays an important role here, where the villi on the apical surface of the RPE is in physical contact with the distal end of the outer segments facilitating their daily phagocytosis within 2 h after light onset (8). It has been estimated that ~80 discs per outer segment are phagocytosed by the RPE per day, accounting for a turnover rate of 10% of the outer segment discs per day (9, 10). This remarkable rate

* This work was supported by Singapore Ministry of Health National Medical Research Council Grant CBRG/069/2014 (to D. L. S.), the Singapore Ministry of Education Tier2 Grant MOE2014-T2-2-018 (to D. L. S.), and National Medical Research Council Grant NMRC/CG/SERI/2013 (to V. A. B.). The authors declare that they have no conflicts of interest with the contents of this article.

[1] To whom correspondence should be addressed: Signature Research Program in Cardiovascular and Metabolic Disorders, Duke-National University of Singapore Graduate Medical School, 8 College Rd., Singapore 169857, Singapore. Tel.: 65-66012172; E-mail: david.silver@duke-nus.edu.sg.

[2] The abbreviations used are: DHA, docosahexaenoic acid; OS, outer rod segment; LPC, lysophosphatidylcholine; BRB, blood-retinal barrier; RPE, retinal pigment epithelium; PFA, paraformaldehyde; IS, inner segment; ONL, outer nuclear layer; BBB, blood-brain barrier; P, postnatal day; PFA, paraformaldehyde; AA, arachidonic acid; ERG, electroretinography.

This is an Open Access article under the CC BY license.

of membrane turnover and RPE phagocytosis is balanced by daily disc regeneration, but an understanding of the cellular process of regeneration of new photoreceptor discs has been poorly understood. Recently, new electron microscopy methodologies have revealed that OS discs are formed through a process of membrane evagination and indicate a highly regulated and ordered process at play in building photoreceptor discs (11–13). Rhodopsin is not only a photoreceptor but is a required structural component for disc membrane formation. Mutations in rhodopsin that reduce rhodopsin levels result in retinitis pigmentosa, a photoreceptor degeneration disease (14, 15). In addition to rhodopsin, phospholipids, including those containing DHA, are major structural components required to build photoreceptor discs, but a biochemical understanding of the origin of these lipids for disc formation is not understood.

We recently identified Major facilitator superfamily domain-containing protein 2a (Mfsd2a) as the primary transporter for the uptake of DHA across the blood-brain barrier (BBB) into brain (16). Mfsd2a transports DHA and other long-chain fatty acids in the chemical form of lysophosphatidylcholine (LPC) in a sodium-dependent manner (16). Mfsd2a is a member of the largest family of secondary transporters and is structurally similar to the bacterial sodium-melibiose transporter (17). In addition to DHA deficiency, Mfsd2a knock-out (KO) mice exhibit severe microcephaly and deficits in learning and memory. Importantly, we have identified humans with homozygous inactivating mutations in Mfsd2a that presented with severe microcephaly and intellectual impairments (18, 19), indicating for the first time that plasma-derived LPCs are required for human brain growth and function. These findings raise the possibility that Mfsd2a is required for DHA uptake in eye. Here we provide evidence that Mfsd2a is critical for DHA transport and accretion by the eye and implicate the transport of LPCs via Mfsd2a expressed at the RPE as important in photoreceptor disc development.

Experimental Procedures

Antibodies—The following antibodies were used in these studies: Cd31 (catalog no. 550274, Pharmingen); Mfsd2a (20); rhodopsin (catalog no. MAB5356, Chemicon/Millipore); ezrin (catalog no. ab4069, Abcam); isolectin GS-IB4 (catalog no. I21411, ThermoFisher Scientific); Iba-1 (catalog no. 019-19741, Wako); Gαt1 (catalog no. sc-389, Santa Cruz Biotechnology); Gβ1 (catalog no. sc-379, Santa Cruz Biotechnology); rhodopsin kinase (Grk1) (catalog no. ab2775, Abcam); Pdeα (catalog no. ab5659, Abcam); Rdh8 (catalog no. ab133738, Abcam); Rpe65 (catalog no. ab13826, Abcam); β-actin (catalog no. A2228, Sigma); and Gapdh (catalog no. sc-32233 Santa Cruz Biotechnology).

Animals—Mfsd2a KO mice were generated as described previously (20). Mfsd2a floxed mice (Mfsd2a$^{tm1a(KOMP)Wtsi}$) were purchased from KOMP Repository where the Mfsd2a exon 3 is floxed by two loxP sites. Mfsd2a floxed mice were then crossed to an FLP recombinant strain (B6.129S4-*Gt*(*ROSA*)*26*$^{Sortm1(FLP1)Dym}$/RainJ, The Jackson Laboratory) to remove the LacZ and neomycin cassette (LL mice). LL mice were then crossed to a cre recombinant strain under the direction of tyrosine kinase *Tek* (Tie2) promoter/enhancer (B6.Cg-Tg(Tek-cre)1Ywa/J, The Jackson Laboratory) to delete Mfsd2a exon 3 specifically in endothelial cells (LLTie2Cre). Mice were maintained on a high energy diet 5LJ5 (PicoLab) containing a total of 11% fat. Pups were weaned at 3 weeks of age. Both male and female mice were used in all experiments, and no gender differences were observed. Mice were anesthetized with a combination of ketamine (20 mg/kg body weight) and xylazine (2 mg/kg body weight) for all experiments (21). Experimental protocols were approved by SingHealth Institutional Animal Care and Use Committee.

Retinal Flat Mounts—Retinal flat mounts were prepared from postnatal day 8 (P8) wild-type (WT) and Mfsd2a-deficient (KO) mice and P9 LL and LLTie2Cre mice and stained as described previously (22). Mice were deeply anesthetized before eyes were enucleated and allowed to fix for 15 min in 4% paraformaldehyde (PFA) at room temperature. Eyes were subsequently transferred to a small Petri dish containing PBS, where an incision was made at the cornea with a sharp blade before cuts were made along the ora serrata. Cornea, lens, and optic nerve were removed, leaving behind eye cups. 4–8 radial incisions reaching ~2/3 of the radius of the eye cup were made using spring scissors to create a "petal" shape. The flattened eye cup was then transferred onto a microscope slide where the retina was carefully separated from the rest of the eye cup. Excess PBS was drained with Kim wipes, and cold methanol was added dropwise onto the surface of the flatted retina. Retinal flat mounts were then transferred into 2-ml tubes containing cold methanol and allowed to fix for an additional 20 min on ice. Methanol was carefully removed and retinal flat mounts were rinsed briefly in PBS before blocking in blocking buffer (0.3% Triton X-100 + 0.2% BSA + 5% normal goat serum in PBS) for 1 h with gentle agitation. Blocking buffer was removed, and retina flat mounts were incubated with Cd31 (1:375) and Mfsd2a (1:250) antibodies diluted in blocking buffer and allowed to incubate at 4 °C overnight with gentle agitation. Fluorescent secondary antibodies were used at a 1:200 dilution before washing and mounting. Images were acquired on Zeiss LSM 710 inverted fluorescence confocal microscope (Carl Zeiss, Singapore). For each retinal flat mount, a total of 36–49 images were taken at ×10 magnification and stitched together using the tile scan function.

Histological Studies—For immunofluorescence staining, P14 wild-type and Mfsd2a KO mice were deeply anesthetized, and eyes were enucleated. Eyes were transferred to a small Petri dish containing 4% PFA, where an incision was made at the cornea with a sharp blade before cuts were made along the ora serrata. Cornea, lens, and optic nerve were removed, leaving behind eye cups. Eye cups were transferred to a 2-ml tube containing 4% PFA and allowed to fix at room temperature for 1–2 h. Eye cups were rinsed briefly in PBS and dehydrated in 10% sucrose for 1 h at room temperature, 20% sucrose for 2–3 h at room temperature, and eventually in 30% sucrose at 4 °C overnight. Eyes were embedded in 1:1 of 30% sucrose/Tissue-Tek O.C.T. Compound (Sakura, CA), and allowed to freeze slowly on dry ice. 12-μm cryosections were prepared using a cryostat (CM1520, Leica) from frozen blocks and processed for immunocytochemistry procedure using antibodies against isolectin GS-IB4 (1:100), Mfsd2a (1:25), ezrin (1:50), and rhodopsin (1:800) and incubated for 1 min in 4′,6-diaminodino-2-phenylindole (DAPI,

1:1000) before washing and mounting. For immunofluorescence staining in Fig. 5*G*, P13 and 5-month-old wild-type and Mfsd2a KO mice were deeply anesthetized as before, and eye cups were prepared as before. 12-μm cryosections were processed for immunocytochemistry procedure using antibodies against ezrin (1:50) and incubated for 1 min in DAPI (1:1000) before washing and mounting. Images were acquired on Zeiss LSM 710 upright fluorescence microscope (Carl Zeiss, Singapore). For hematoxylin and eosin (H&E) staining, P13, 4.5-month-old, and 16-month-old wild-type and Mfsd2a KO mice and 4-month-old LL and LLTie2Cre mice were deeply anesthetized as before. Eyes were enucleated and placed immediately in Perfix solution (4% paraformaldehyde, 20% isopropyl alcohol, 2% trichloroacetic acid, 2% zinc chloride) at room temperature for 48 h. Whole eyes were processed and embedded in paraffin. 5-μm sections were prepared using a microtome (RM2255, Leica), and H&E staining was performed. Images were taken on a DMi8 fluorescent microscope (Leica). For each eye section, a total of 200–300 images were taken at ×40 magnification and stitched together using the tile scan function. Lengths of outer segments (OS) and inner segments (IS) of the photoreceptor were measured, and the ratio of OS/OS+IS was calculated on ImageJ. Outer nuclear layer (ONL) quantification in 16-month-old mice was carried out by quantifying the number of nuclei across the ONL at 250-μm intervals from the optic nerve. Graphs and statistics analysis were done on GraphPad Prism.

Western Blotting—To prepare tissues for Western blot analysis, mice were deeply anesthetized as before, and the eyes were enucleated. Eyes were transferred to a small Petri dish containing cold PBS, where an incision was made at the cornea with a sharp blade before cuts were made along the ora serrata. Cornea, lens, and optic nerve were removed, leaving behind eye cups. The retina was removed carefully with blunt forceps, leaving behind eye cups without retina (RPE). Excess PBS was drained with Kim wipes, and tissues were flash-frozen immediately in liquid nitrogen. Whole eyes, retina, and RPE (eye cups without retina) were ground with a cell pellet homogenizer (VWR) in RIPA buffer with EDTA-free cOmplete protease inhibitor mixture (Roche Applied Science), phosphatase inhibitor mixture 2 (catalog no. P5726, Sigma), and phosphatase inhibitor mixture 3 (catalog no. P0044, Sigma) on ice. Protein samples were separated by SDS-PAGE, transferred to nitrocellulose membranes (Bio-Rad), and incubated overnight with antibodies at 1:1,000 dilution and GAPDH and β-actin at 1:5,000 dilution. 2 μg of whole eye lysate was used for Fig. 7*C*, and 30 μg of whole eye lysate was used for Fig. 7*D*.

Fundus Fluorescein Angiography—Fundus fluorescein angiography was performed as described previously (21). Briefly, 3-month-old wild-type and Mfsd2a KO mice were anesthetized and injected with 10% sodium fluorescein dye (0.01 ml/5–6 g of body weight).

Sulfo-NHS-Biotin—Intracardiac perfusion of Sulfo-NHS-Biotin was carried out as described previously (23) with modifications. P22 to P24 wild-type and Mfsd2a KO mice were anesthetized and perfused with 10–30 ml of Sulfo-NHS-biotin (catalog no. 21217, Thermo Scientific) in PBS, followed by 2% PFA in PBS. Eyes were enucleated and post-fixed in 1% PFA at 4 °C for 4–6 h prior to retina dissection. Eyes were transferred to a small Petri dish containing cold PBS, where an incision was made at the cornea with a sharp blade before cuts were made along the ora serrata. Cornea, lens, and optic nerve were removed, leaving behind eye cups. Retinal flat mounts were prepared as described before. Retinal flat mounts were transferred carefully into a 2-ml tube and incubated with GS-isolectin (1:100 dilution) and Texas Red streptavidin (catalog no.: SA-5006, Vector Laboratories) diluted in PBS + 0.5% Triton X-100 + 0.1 mM $CaCl_2$ with (PBSTC) with 10% normal goat serum at 4 °C overnight. Retinal flat mounts were washed with PBSTC and mounted. Images were acquired on Zeiss LSM 710 inverted fluorescence confocal microscope (Carl Zeiss, Singapore).

10-kDa Dextran Injections—Retro-orbital injection of lysine-fixable 10-kDa dextran conjugated to tetramethylrhodamine (Invitrogen) (50 mg/ml in saline) was carried out in P21 wild-type and Mfsd2a KO mice at a dose of 2 mg/20 g of body weight. 2 h post-injection, mice were anesthetized, and brains were harvested and fixed in 4% PFA in PBS at 4 °C overnight. Brains were then dehydrated in 30% sucrose before freezing in Tissue-Tek O.C.T. Compound (Sakura) on dry ice. 20-μm cryosections were prepared using a cryostat (CM1520, Leica) from frozen blocks and processed for the immunocytochemistry procedure using antibodies against Cd31 (1:100) and incubated for 1 min in DAPI (1:1,000) before washing and mounting. Images were acquired on Zeiss LSM 710 upright fluorescence microscope (Carl Zeiss, Singapore).

Lipidomic Analysis—Tissue lipid analysis was carried out as described previously (18). Wild-type and Mfsd2a KO mice aged 7–8 weeks or LL and LLTie2Cre mice aged 7 weeks were deeply anesthetized and perfused transcardially with 30 ml of saline. Eyes were enucleated; optic nerve was removed and immediately frozen with liquid nitrogen until extraction. Lipid extraction was followed by the chloroform/methanol method. Samples were randomized for injection into a liquid chromatography-tandem mass spectrometry (LC-MS/MS) instrument. Every sample was injected twice for analysis by two methods due to the high number of multiple reaction monitoring transitions to monitor. Two quality controls (one for each method) and two blanks (one for each method) were injected after every six sample injections to avoid carryover. The stability of signal throughout the analysis was monitored by regular injection of a quality control sample (chromatographic analysis was undertaken on a 1290 Liquid Chromatography System, Agilent Technologies) using a Kinetex HILIC stationary phase (150 × 2.1 mm, 2.6 μM, 100 Å; Phenomenex). Gradient elusions were performed with solvents A (50% acetonitrile + 50% 25 mM ammonium formate buffer, pH 4.6) and B (95% acetonitrile + 5% 25 mM ammonium formate buffer, pH 4.6), with a gradient range from 75 to 25% solvent B in 6 min, 90 to 10% solvent B in 1 min, 0.1 to 99.9% solvent B in 0.1 min, followed by 0.1 to 99.9% solvent B for 3 min (total run time of 10.1 min). Under these conditions, phospholipid species elute in ~4.9 min with a flow rate of 0.5 ml/min. Phospholipids were quantified using multiple reaction monitoring on a 6460 triple-quadruple mass spectrometer (Agilent Technologies) with gas temperature of 300 °C, gas flow of 5 liters/min, sheath gas flow of 11 liters/min, and capillary voltage of 3,500 V. Quantification data were

extracted using MassHunter Quantitative Analysis (QQQ) software, and data were manually curated to ensure correct peak integration. Areas under the curve for the extracted ion chromatogram peaks for each multiple reaction monitoring transition and lipid species were normalized to an internal standard and total weight of eye samples used in the lipid extraction. Isotope correction was then done on all lipid species. Graphs and statistics analysis were done on GraphPad Prism.

In Vivo Transport of Radiolabeled LPC [^{14}C]DHA—*In vivo* transport assay was carried out as described previously (16) with some modifications. To prepare the LPC/DHA mixture for *in vivo* transport assay, 6 μCi of LPC [^{14}C]DHA (specific activity, 50 μCi/mmol, American Radiolabeled Chemicals) solubilized in ethanol/toluene was added to unlabeled LPC/DHA in chloroform (Romega® LPC/DHA, a kind gift from Arctic Nutrition, Ørsta, Norway) and completely dried under nitrogen gas. The LPC/DHA mixture was then solubilized in 1.4 ml of 12% fatty acid-free BSA (Sigma) in 150 mM NaCl to a final concentration of 14 mM. Wild-type and Mfsd2a KO mice at 4 weeks of age were intravenously injected with 100 μl of 14 mM radiolabeled LPC [^{14}C]DHA-BSA complex. At 18 h post-injection, mice were deeply anesthetized and perfused for 5 min with PBS containing 0.5% BSA to remove blood and lipid tracer bound to brain, eye, and heart vasculature. Eyes are small relative to brain; hence, an 18-h timeline was used to maximize tracer uptake for detection. Brain and heart tissues were collected whole for lipid extraction. Eyes were transferred to a small Petri dish containing cold PBS, where an incision was made at the cornea with a sharp blade before cuts were made along the ora serrata. Cornea, lens, and optic nerve were removed, leaving behind eye cups. Excess PBS was drained with Kim wipes, and tissues were weighed and kept on ice. For lipid extraction, similar amounts of tissues were homogenized in chloroform/methanol. Lipids from the organic phase were mixed with scintillant and scintillation counted. Graphs and statistics analysis were done on GraphPad Prism.

Plastic Sections and Scanning Electron Microscopy—P13, 3-month- and 4-month-old wild-type and Mfsd2a KO mice were anesthetized, and eyes were enucleated and placed immediately in a small Petri dish containing fixative (2% PFA and 2% glutaraldehyde in 0.1 M cacodylate buffer, pH 7.4). An incision was made at the cornea with a sharp blade before cuts were made along the ora serrata. Cornea and lens were removed, leaving behind eye cups. Eye cups were cut into two parts, close to the optic nerve. Trimmed eyecup pieces were transferred to fresh fixative and kept at 4 °C overnight. Following fixation, eyes were post-fixed in 2% osmium tetroxide and potassium ferrocyanide (Electron Microscopy Sciences, Hatfield, PA) for 2 h. Samples were rinsed and dehydrated in a graded series of ethanol and embedded in Araldite. Ultra-thin sections of 80–100 nm were collected on copper grids and viewed on a Zeiss Merlin Field-Emission Scanning Electron Microscope (Carl Zeiss Microscopy, Oberkochen, Germany). Images were captured using an annular Scanning Transmission Electron Microscope (aSTEM) detector at acceleration voltage of 30 kV.

Electroretinography—Electroretinography was performed as described previously (21). Briefly, wild-type and Mfsd2a KO mice were dark-adapted overnight (12 h), and all recordings (30 min for each animal) were carried out under dim red light. A gold-cup electrode (Grass-Telefactor, West Warwick, RI) served as the reference electrode, which was placed in the mouths of the mice. A silver-silver chloride electrode (Grass-Telefactor, West Warwick, RI) which served as the ground electrode, was placed in the tail. Measurements were taken at stimulus intensities of −3.3 to 1.0 log candela·s/m2 in 0.3-log unit increments.

Gene Array and Pathway Analysis—To prepare tissues for gene array, P13 wild-type and Mfsd2a KO mice were deeply anesthetized, and eyes were enucleated. Eyes were transferred to a small Petri dish containing cold PBS, where an incision was made at the cornea with a sharp blade before cuts were made along the ora serrata. Cornea, lens and optic nerve were removed, leaving behind eye cups. Excess PBS was drained with Kim wipes and tissues were flash-frozen immediately in liquid nitrogen. Eye cups were ground with a cell pellet homogenizer (VWR) on ice in TRIzol (Roche Applied Science). RNA was extracted and purified with RNeasy mini kit (Qiagen) and quantified by Nanodrop. Equal amounts of RNA from six wild-type eye cups were pooled for the wild-type sample, or 6 Mfsd2a KO eye cups were pooled for the Mfsd2a KO sample, and RNA integrity was verified using Bioanalyzer (Agilent Technologies). Microarray profiling was done on pooled samples with an RNA integrity cutoff of 7.0 using Mouse 430 2.0 arrays (Affymetrix). Filtered gene list (genes with maximum expression in KO or WT >50 and fold-change >1.25 or <0.75) was analyzed using Ingenuity Pathway Analysis software to identify significantly altered canonical pathways and predicted activation or inhibition of upstream inhibitors of Mfsd2a. Microarray data are available at Geo Profiles (www.ncbi.nlm.nih.gov), accession number GSE77403. Target validation using quantitative-PCR was performed on selected targets with primers indicated in Table 2.

Statistical Analysis—Statistical differences of DHA and AA levels, uptake of LPC [^{14}C] DHA in tissues, and histological analyses between genotypes were calculated using an unpaired Student's *t* test. A $p < 0.05$ was considered to be significant.

Results

Mfsd2a Is Expressed in Retinal Vessels and RPE—Because Mfsd2a is specifically expressed in the endothelium of the BBB, we first tested its expression in the retinal vasculature. The murine retina and retinal vasculature develop postnatally with vessels growing from the inner ganglion layer at postnatal day 0 down to the outer plexiform layer by postnatal day 11 before vascularizing the inner plexiform layer by postnatal day 15. Immunolocalization of Mfsd2a in retinal flat mounts indicated that it is expressed in mature capillaries of the eye that form the BRB (Fig. 1*A*) but is absent at tip cells from the leading edge of the developing vasculature (Fig. 1*A*). This finding is consistent with a previous report that utilized our antibody as demonstrated here (24). In addition to expression in the endothelium of the BRB, Mfsd2a was also expressed in RPE (Fig. 1, *B* and *C*). Western blot confirmed these findings, but additionally indicated that Mfsd2a is expressed at much higher levels in RPE (eye cups excluding retina) than in retina (Fig. 1*D*). Mfsd2a in the retina appeared as two diffuse bands, but as a single band in

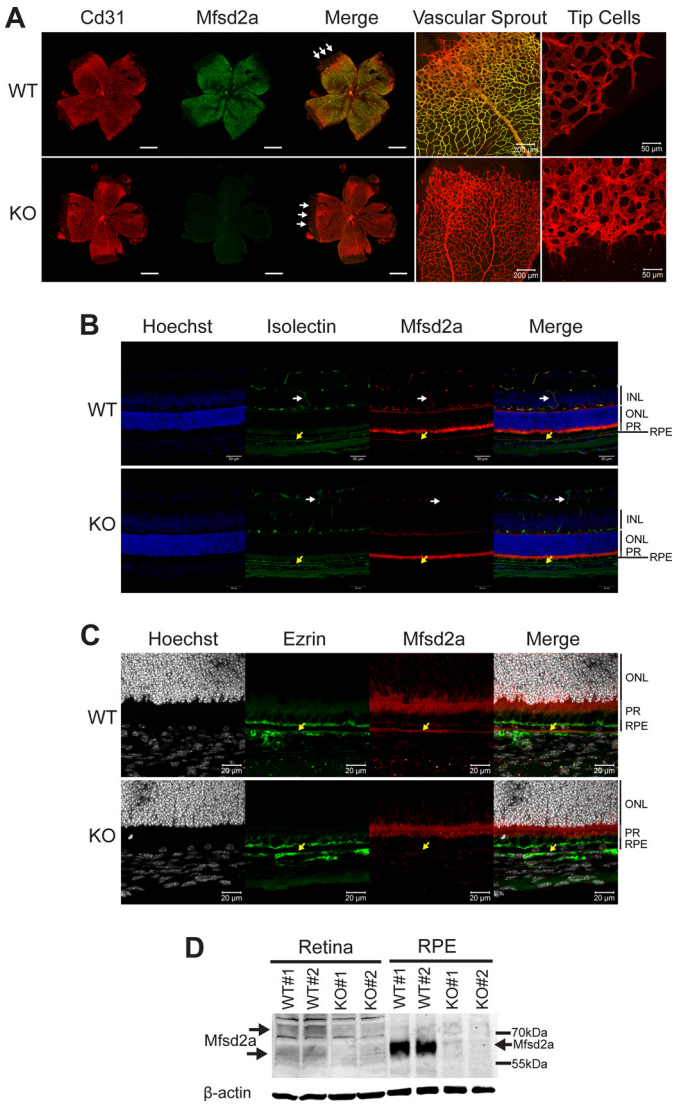

FIGURE 1. **Mfsd2a is expressed in retinal vessels and RPE.** *A,* immunolocalization of Mfsd2a in capillaries of the developing eye. Retinal whole mounts were prepared from postnatal day 8 wild-type (*WT*) and Mfsd2a deficient (*KO*) mice and stained for the endothelial cell marker Cd31 and Mfsd2a. Mfsd2a KO served as a negative control for Mfsd2a antibody specificity. Endothelial tip cells are seen at the leading edge of the growing vasculature sprouts (*white arrows*). Mfsd2a is shown to be expressed only in mature capillaries but is absent in tip cells. *WT*, $n = 4$; *KO*, $n = 4$; *scale bar* = 1 mm. *B,* cross-sections of eyes of postnatal day 14 (*P14*) mice were stained for isolectin, an endothelial marker, Mfsd2a, and Hoechst (a nuclear stain). Co-expression is seen in the capillaries (*white arrow*) and RPE (*yellow arrow*). Autofluorescence is observed in photoreceptor outer segments. WT, $n = 5$; KO, $n = 5$; *scale bar,* 50 μm. *C,* to confirm Mfsd2a expression in the RPE, eye sections from P14 mice were stained for ezrin, an apical and basolateral membrane marker in RPE, and Mfsd2a, and Hoechst (a nuclear stain). Co-expression is seen at the basolateral membrane (*yellow arrow*). Autofluorescence is observed in photoreceptor outer segments. *WT*, $n = 5$; *KO*, $n = 5$; *scale bar,* 20 μm. *D,* representative Western blot of Mfsd2a expression in 80 μg of retina and 8 μg of RPE (eye cup without retina) in 8-week-old mice. Mfsd2a is more abundantly expressed in RPE relative to the retina. β-Actin served as a loading control. *WT*, $n = 4$; *KO*, $n = 4$. *INL,* inner nuclear layer; *PR,* photoreceptor.

the RPE (Fig. 1*D*). The two molecular weight species observed for Mfsd2a in the retina have been observed previously for Mfsd2a in liver and in overexpression studies in HEK293 cells and explained by alternative glycosylation (18, 20). The single molecular weight species of Mfsd2a detected in RPE is similar to the molecular weight of Mfsd2a reported for brain (16).

Mfsd2a Is Not Critical for the Integrity of the BRB—It has recently been reported that Mfsd2a is critical for the formation and function of the BBB in mice, where mice deficient in Mfsd2a exhibited increased vascular permeability in embryonic and adult brain as determined by diffusion of fluorescent dextran probes from circulation into the surrounding brain parenchyma (25). Moreover, that study reported that decreased barrier function of the BBB was the result of increased transcytosis, not disruption of tight junctions, a phenotype observed in mice with pericyte deficiency (26–28). We therefore were compelled to determine whether Mfsd2a plays an important role in the maintenance of the BRB. Fluorescein angiography, a standard method to determine BRB integrity, performed on adult retinas of living Mfsd2a KO and control mice failed to reveal leakiness of retinal vessels (Fig. 2*A*). To determine whether leakiness might occur in younger mice, we examined retinal vascular integrity in postnatal day 22–24 (P22–P24) mice. This time point was chosen because it is the developmental stage at which eye development is completed. Because animals are too small for fluorescein angiography, we made use of a Sulfo-NHS-biotin cross-linker (molecular weight, 443.43 g/mol), which has previously been developed as a sensitive method for measuring BRB and BBB integrity (23). P22–P24 mice underwent intracardiac perfusion of Sulfo-NHS-biotin cross-linking agent, and retinal whole mounts were stained for covalent biotin adducts. Consistent with findings from fluorescein angiography, there was an absence of biotin leakage out of the retinal vasculature in Mfsd2a KO mice (Fig. 2*B*). Given the report that Mfsd2a KO mice have leaky BBB, brains from Sulfo-NHS-biotin injected mice were examined for integrity of the BBB. Remarkably, there was no evidence of increased Sulfo-NHS-biotin leakiness from brain capillaries into surrounding parenchyma of Mfsd2a KO relative to wild-type control mice regardless of brain region (Fig. 2*C*). It is important to note that in rare instances we did observe leakiness in both Mfsd2a KO and wild-type mice. To further confirm these negative findings, Mfsd2a KO and wild-type mice were intravenously injected with 10-kDa fluorescent dextran tracer, same as reported previously (25), but again there was no evidence of BBB leakage of this tracer into brain parenchyma of Mfsd2a KO mice (Fig. 2*D*). These data indicate that there is no disruption of BRB and BBB integrity in Mfsd2a KO mice used in these studies.

Mfsd2a Is Required for Normal DHA Accretion in Eye—Because Mfsd2a is the primary route for DHA uptake in the brain and Mfsd2a KO mice are DHA-deficient (16), we tested whether eyes of Mfsd2a KO mice are indeed DHA-deficient. To carry out this goal, a comprehensive lipidomic analysis of eyes by mass spectrometry was performed on wild-type and Mfsd2a KO mice as reported previously for the analysis of brain from Mfsd2a KO mice (16). Importantly, total steady-state levels of DHA-containing phospholipids, but not other long chain fatty acids in phospholipids, from eyes of Mfsd2a KO mice were decreased by more than 40% relative to wild-type mice (Fig. 3*A*). Moreover, levels of AA in phospholipids of eyes of Mfsd2a KO mice were moderately increased (Fig. 3*A*), which is commonly observed in models of dietary DHA deficiency (29). In addition, the levels of phospholipids containing fatty acid spe-

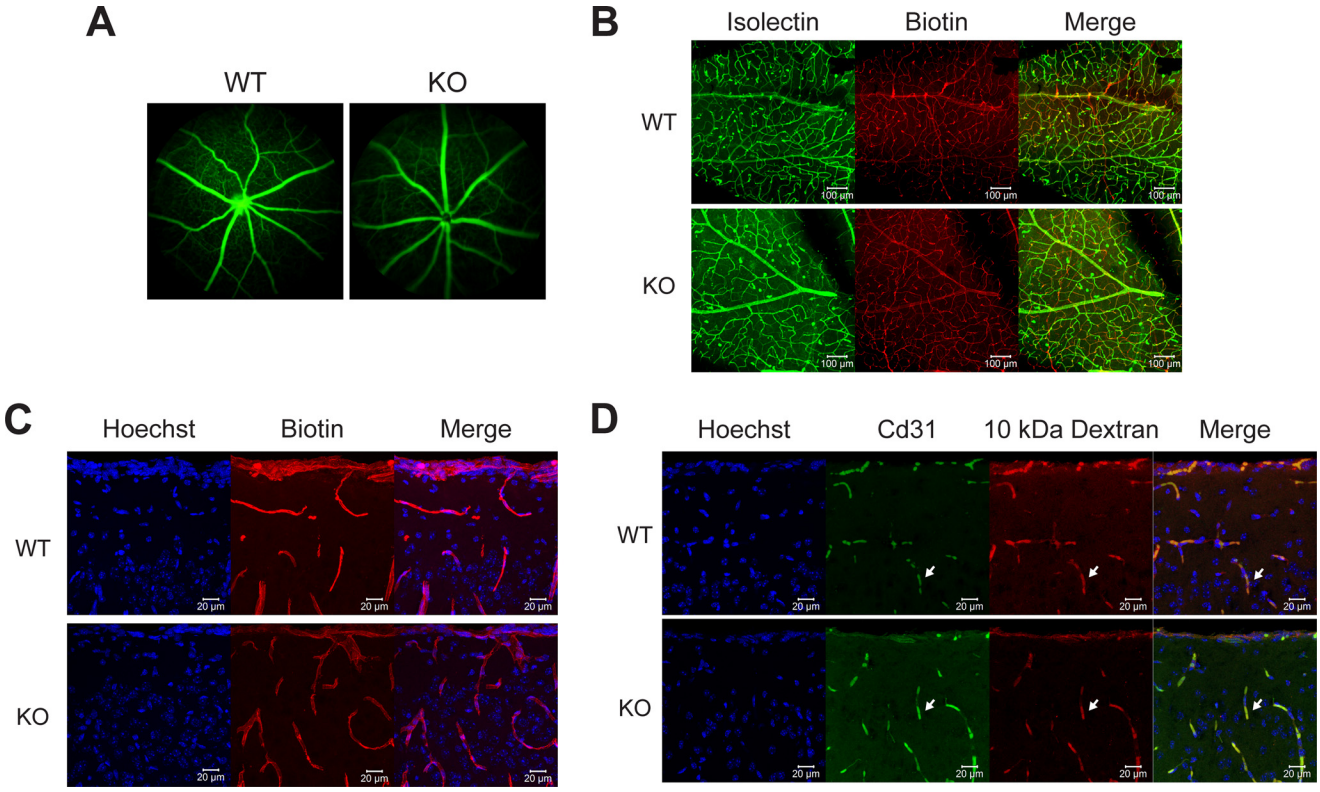

FIGURE 2. **BRB and BBB are not leaky in Mfsd2a KO mice.** *A,* representative image from fundus fluorescein angiography performed on 3-month-old wild-type and Mfsd2a KO mice. Fluorescein tracer was not observed outside of capillaries in Mfsd2a KO retina indicating intact BRB. *WT*, $n = 5$; *KO* $n = 5$. *B,* intracardiac perfusion of Sulfo-NHS-Biotin was carried out on P22–P24 mice, and retinal flat mounts were stained for biotin adducts and isolectin (an endothelial marker). No biotin adducts were observed outside of retinal capillaries, indicating intact BRB. *Scale bar,* 100 μm. *WT*, $n = 2$; *KO*, $n = 2$. *C,* brains harvested from animals in *B* were sectioned and stained for biotin adducts and Hoechst (a nuclear stain). No biotin adducts were observed outside of brain capillaries in the brain cortex, indicating intact BBB. *WT*, $n = 2$; *KO*, $n = 2$, *scale bar,* 20 μm. *D,* 10-kDa dextran tracer was injected intravenously into P21 mice, and brains were harvested without perfusion 2–3 h post-injection. Brain sections were stained for the endothelial cell marker Cd31 and Hoechst (a nuclear stain). Co-expression of Cd31 and 10-kDa dextran tracer is seen in the capillaries (*white arrow*). No tracer was observed outside of brain capillaries in the brain cortex, indicating intact BBB. *Scale bar,* 20 μm. *WT*, $n = 2$; *KO*, $n = 2$.

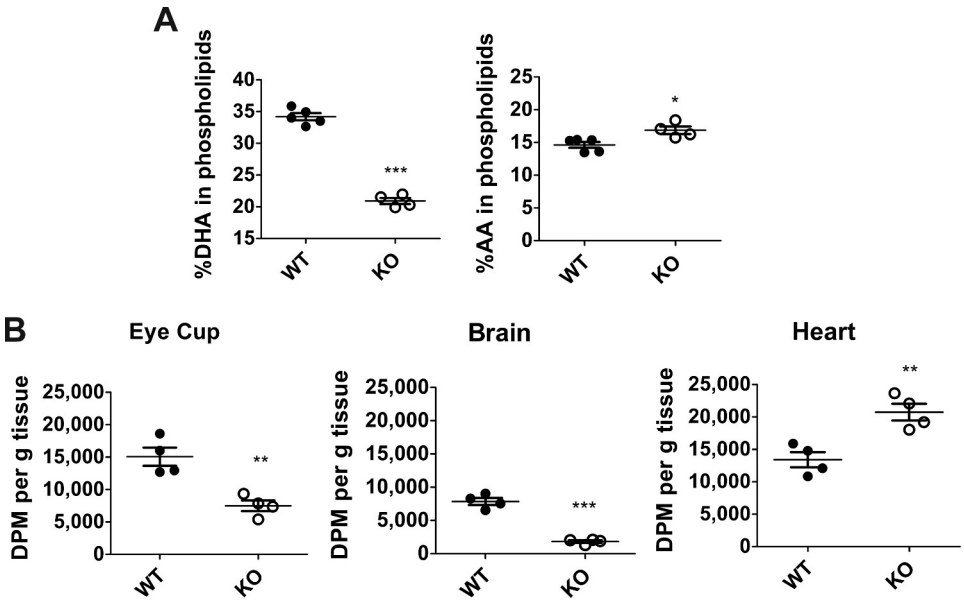

FIGURE 3. **Eyes of Mfsd2a KO mice are DHA-deficient with decreased uptake of radiolabeled LPC-[^{14}C]DHA.** *A,* comprehensive lipidomic analysis of whole eyes from 8-week-old mice. Total DHA and arachidonic acid (*AA*) levels in eye phospholipids are shown. *WT*, $n = 5$; *KO*, $n = 4$. ***, $p < 0.0001$; *, $p = 0.0167$. *B,* 4 week old mice were injected intravenously with the same dose of LPC-[^{14}C]DHA. Eye cup, brain, and heart were collected 18 h post-injection for lipid extraction, and DPM was quantified using scintillation counting. Uptake is expressed as mean ± S.E. *WT*, $n = 4$; *KO*, $n = 4$. ***, $p < 0.0001$; **, $p < 0.006$.

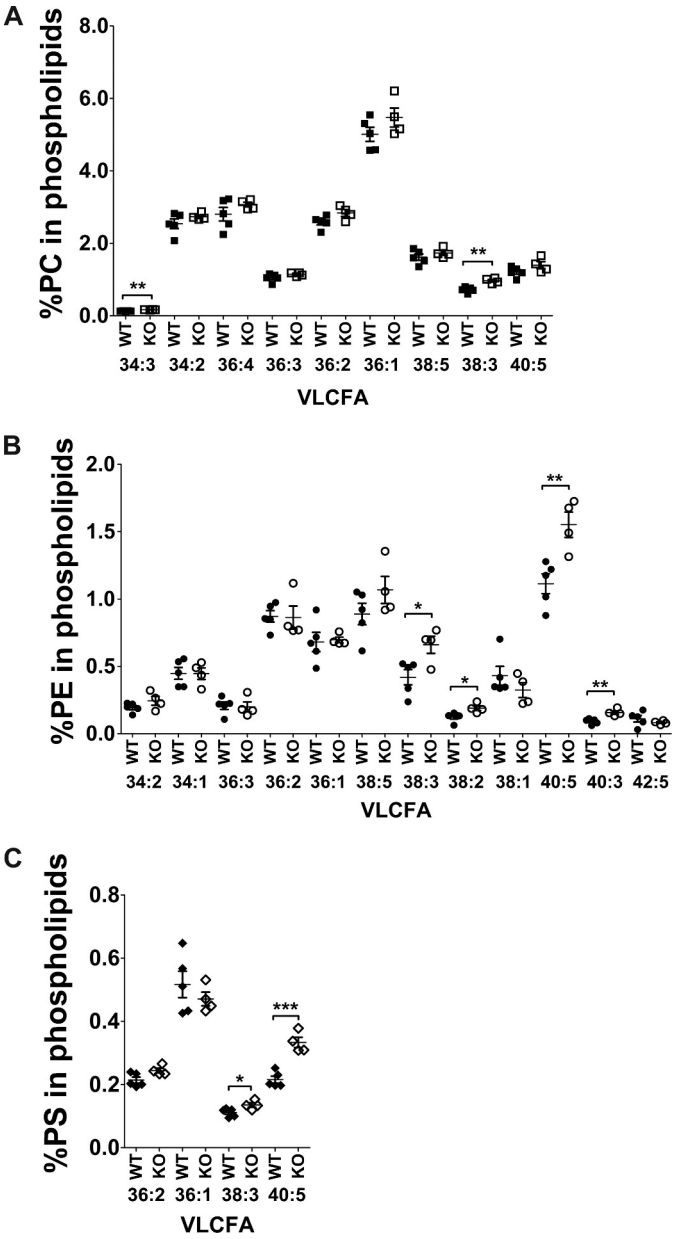

FIGURE 4. **Comprehensive lipidomic analysis of phospholipid pools containing unsaturated fatty acids of whole eyes from 8-week-old wild-type and Mfsd2a KO mice.** Percentage of very long chain unsaturated fatty acid (*VLCFA*) species in phosphatidylcholine (*PC*) (*A*), phosphatidylethanolamine (*PE*) (*B*), and phosphatidylserine (*PS*) (*C*) in eye phospholipids are shown. Fatty acid identity is designated as number of carbons/number of double bonds; *e.g.* 40:5 indicates a phospholipid with 40 carbons and 5 double bonds. *WT*, $n = 5$; *KO*, $n = 4$. ***, $p < 0.001$; **, $p < 0.01$; **, $p < 0.05$.

cies of 40:5, 40:3, 38:3, and 38:2 were also moderately increased in Mfsd2a KO eyes (Fig. 4).

To determine whether decreased DHA in the eyes of Mfsd2a KO mice is due to reduced LPC/DHA transport into the eye, an *in vivo* LPC/DHA transport assay was carried out as developed previously for brain (16). In this assay, Mfsd2a KO and wild-type mice were intravenously injected with similar concentrations of radiolabeled 1-docosahexaenoyl 2-lysophosphocholine (LPC-[^{14}C]DHA), despite that Mfsd2a KO mice have significantly reduced body weights (~50% of wild type) and thus received a significantly higher amount of LPC-[^{14}C]DHA than wild-type controls (~50% more than wild type). At 18 h post-injection, mice were perfused, and eyes, hearts, and brains were collected and analyzed. Brain served as a positive control where it is established that Mfsd2a is required for LPC/DHA uptake, whereas heart, which does not express Mfsd2a, served as a negative control and indicates an overall dose taken up by mice during the experiment. Indeed, Mfsd2a KO mice exhibited a 50% reduction of LPC-[^{14}C]DHA uptake in eyes (Fig. 3*B*), which is likely an underestimate of the real difference given that Mfsd2a KO mice received a higher dose per g of body weight than wild-type mice. As expected, LPC-[^{14}C]DHA uptake in brains of Mfsd2a KO mice was reduced by 77% relative to wild-type controls. Conversely, uptake in the heart of knock-out mice was not decreased but was increased by 55% consistent with a 50% increase in injected dose in Mfsd2a KO mice relative to wild-type mice. Taken together, these findings indicate that, like in brain, Mfsd2a is a major transporter for DHA accretion in the eye.

Mfsd2a Deficiency Reduces Photoreceptor Segment Length—We next sought to determine whether there are any anatomical and functional consequences to Mfsd2a deficiency in the eye. To compare the retina anatomy from both wild-type and Mfsd2a KO mice at 4 months of age, plastic sections were prepared, and toluidine blue staining was used to visualize retina layers. The overall size of the eye was found to be reduced in adult Mfsd2a KO mice relative to wild-type controls. On closer examination, the ONL, which harbors the cell bodies of photoreceptor cells, from Mfsd2a KO mice appeared disorganized with the absence of a clear limiting membrane between the ONL and inner segment and visibly reduced amounts of nuclei (Fig. 5*A*). Moreover, the OS, the location of photoreceptors and DHA, from Mfsd2a KO eyes appeared disorganized and thinner relative to wild-type eyes (Fig. 5*A*). Typically, the OS and RPE are in close contact, as seen in wild-type eyes, but gaps in this area between the OS and RPE in Mfsd2a KO eyes are evident (Fig. 5*A*).

To examine the ultrastructure of Mfsd2a KO eyes, scanning electron microscopy (EM) was carried out on eyes from 4-month-old mice. EM images indicated that OS from Mfsd2a KO mice appeared disorganized (Fig. 5*B*). In addition, the RPE from Mfsd2a KO mice appeared enlarged (Fig. 5*B*). Upon closer inspection of the apical membranes of the RPE, villi of wild-type RPE are extended and in close contact with OS (Fig. 5*B*). However, villi of RPE from Mfsd2a KO mice appeared to have collapsed and to lack close interactions with OS (Fig. 5*B*). For basal infoldings, the villi on the basal membrane of the RPE appeared to be edematous in Mfsd2a KO mice (Fig. 5*B*).

Given that the RPE is the primary site of expression in eye (Fig. 1*D*), and RPE forms during embryogenesis but OS during postnatal development, raised the possibility that the RPE and retina phenotypes described here might occur early in postnatal development. Indeed, Western blot analysis indicated that Mfsd2a is expressed in the RPE as early as embryonic day 18.5 (Fig. 5*C*). To determine whether OS and RPE phenotypes were present before the onset of vision and light exposure to the retina, we examined eyes at P13, a developmental time point in mice before eyes open and retina photoreceptors are fully

developed. In contrast to ONL loss in adult Mfsd2a KO mice, ONL length appeared normal in retinas of P13 Mfsd2a KO mice (Fig. 5, *A* and *D*), indicating that reduced ONL numbers seen in older Mfsd2a KO mice are due to photoreceptor degeneration and loss (Fig. 5). However, similar to adult Mfsd2a KO mice, significantly reduced OS lengths are seen as early as P13 in Mfsd2a KO mice (Fig. 5, *D* and *E*). Upon closer examination by EM, photoreceptor discs in eyes of Mfsd2a KO mice appeared disorganized and misfolded (Fig. 5*F*). In addition, villi at the RPE apical membrane of Mfsd2a KO appeared thickened,

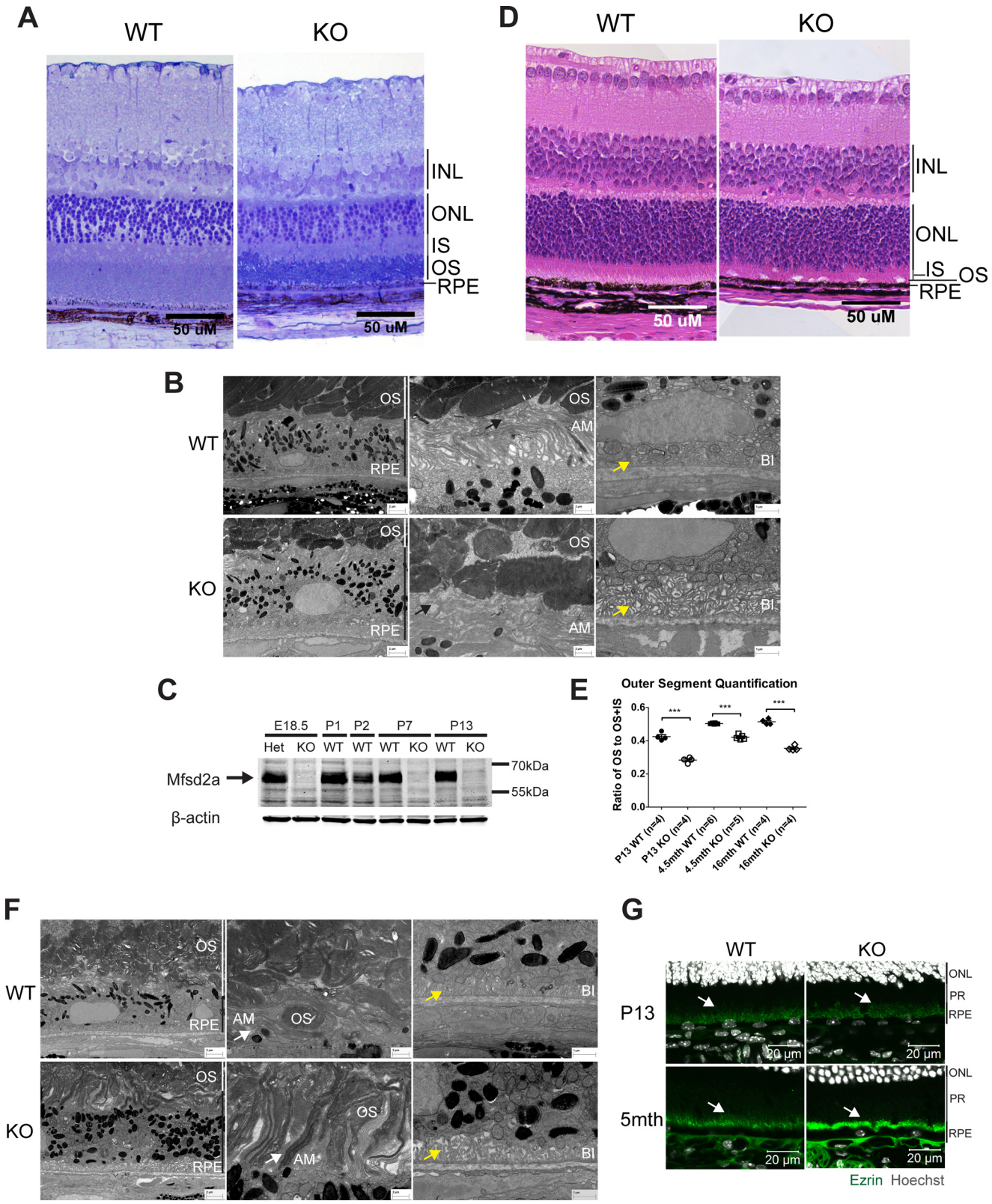

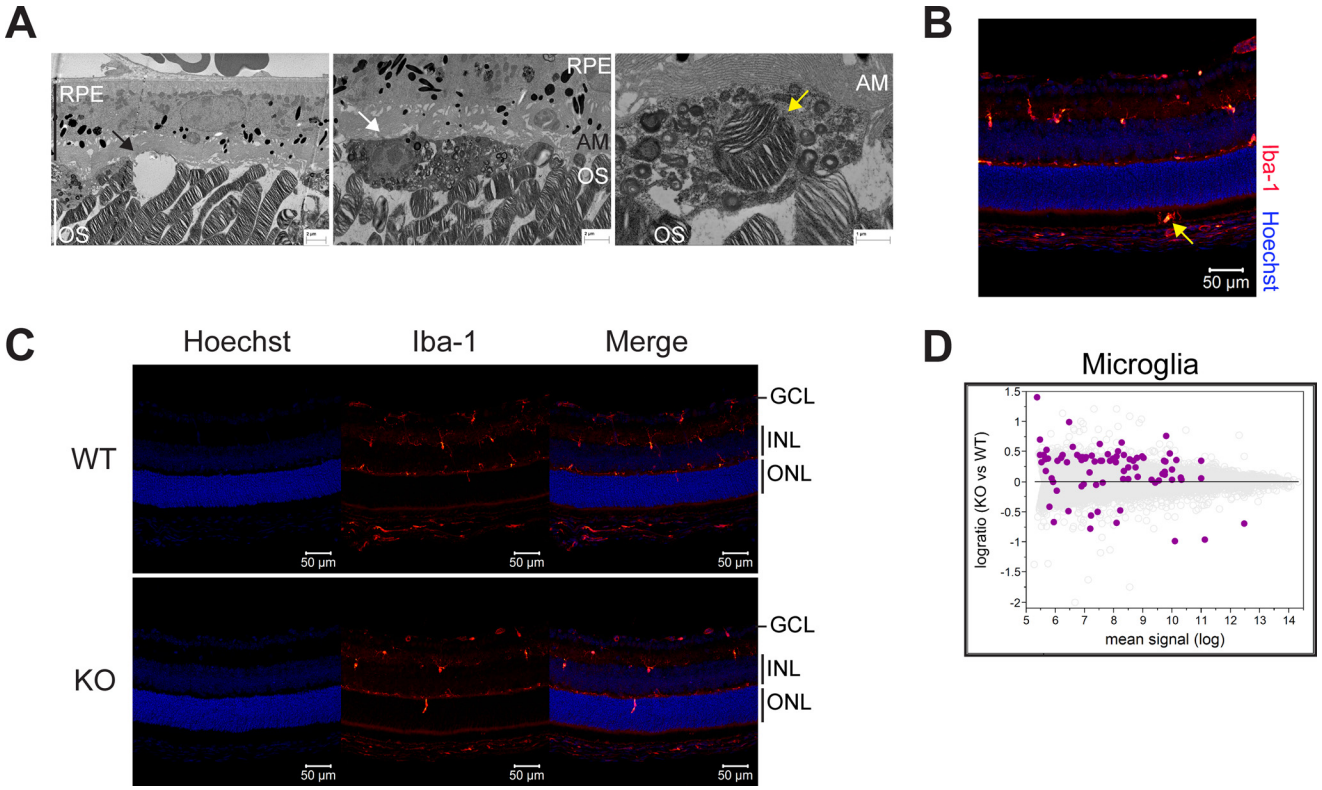

FIGURE 6. **Mfsd2a deficiency results in activated microglia and up-regulation of microglia/interferon pathway.** *A,* S.E. images from 3-month-old mice show large gaps in the subretinal space (*black arrow*). *Scale bar,* 2 μm. The *middle panel* shows a phagocytic cell (*white arrow*). *Scale bar,* 2 μm. The *far right panel* shows an example of a phagocytic cell containing OS discs in an endosome (*yellow arrow*). *Scale bar,* 1 μm. *AM,* apical membrane; *BI,* basal infoldings. *B,* immunolocalization of the microglia/macrophage marker Iba-1 was performed on eye sections from P14 mice. Iba-1-positive cells, which normally reside in the inner eye, were found in the subretinal space (*yellow arrow*). *Scale bar,* 50 μm. *C,* immunolocalization of Iba-1 as done in *B*. Iba-1-positive cells appeared rounder and less ramified compared with WT, indicative of an activated state. *Scale bar* = 50 μm. *WT*, $n = 5$; *KO*, $n = 5$. *GCL,* ganglion cell layer; *INL,* inner nuclear layer. *D,* gene microarray analysis from P13 eye cups of WT and Mfsd2a KO mice. An MA plot, which is used to visualize intensity-dependent ratio of raw gene microarray data, indicated that the third highest ranked pathway that was up-regulated in Mfsd2a KO eyes was the microglia/interferon pathway. *Purple dots* represent individual targets in this pathway over the background of expressed genes.

although basal infoldings appeared edematous (Fig. 5*F*). Immunolocalization of ezrin, which is a marker for RPE apical villi, in wild-type RPE showed the expected organized hair-like villi structures at P13 and 5 months of age (Fig. 5*G*). In contrast, RPE apical villi of both P13 and 5-month-old Mfsd2a KO mice were disorganized (Fig. 5*G*). Collectively, these findings indicate an early onset of reduced OS length, disorganization of OS discs, and alterations in RPE morphology, suggesting potential defects in disc biogenesis.

In some EM images of Mfsd2a KO but not wild-type eyes, large gaps in the subretinal space were noted along with phagocytic cells containing OS discs in endosomes (Fig. 6*A*, also seen in Fig. 5, *A* and D), suggestive of microglia in the outer retina. Consistent with this interpretation, immunolocalization of Iba-1, a marker for microglia/macrophage, showed that Iba-1-positive cells, which normally reside in the inner eye, were found both in the ONL and subretinal space in Mfsd2a KO eyes (Fig. 6, *B* and *C*). Moreover, Iba-1-positive cells in Mfsd2a KO eyes appeared rounded and less ramified than seen in wild-type eyes (Fig. 5, *B* and *C*), indicative of an activated state (30). Supportive of this conclusion, microarray analysis from eye cups of P13 Mfsd2a KO and wild-type controls indicated

FIGURE 5. **Mfsd2a deficiency results in shortened and disorganized OS and swollen RPE.** *A,* plastic sections of eyes of 4-month-old mice. Toluidine blue staining was carried out to visualize the layers, as indicated to the *right* of the figure. OS of Mfsd2a KO mice appear thinner and more disorganized, with some ONL loss, although the other retinal layers appear comparable with wild type. *Scale bar,* 50 μm. *B,* S.E. images from 4-month-old mice show the disorganization of the OS in Mfsd2a KO mice, and RPE appears swollen. *Scale bar,* 2 μm. The *middle panel* shows that villi of wild-type RPE is in close contact with the OS (*black arrow*), but villi of Mfsd2a KO appears collapsed and not interacting with OS (*black arrow*). *Scale bar,* 2 μm. The *far right panel* is of the basal membrane of the RPE. Edema was seen at the basal infoldings of Mfsd2a KO RPE but not in wild-type RPE (*yellow arrow*). *Scale bar,* 1 μm. *C,* representative Western blot of Mfsd2a expression in RPE. Mfsd2a is expressed in the RPE as early as E18.5. Mfsd2a KO RPE was used as negative control for some age groups. The age in postnatal days is indicated. *D,* H&E staining of eyes of P13 mice was carried out to visualize the layers, as indicated to the *right* of the figure. OS of Mfsd2a KO mice appear thinner, although other retinal layers appear comparable with wild type. *Scale bar,* 50 μm. *WT*, $n = 4$; *KO*, $n = 4$. *E,* ratio of OS to OS + IS was quantified in eyes of P13 and 4.5- and 16-month-old mice. OS are shorter in eyes of Mfsd2a KO mice, as early as age P13, indicating an early onset of reduced OS length. Number of mice per age group used as indicated in *graph*. ***, $p < 0.0001$. *F,* S.E. images from age P13 mice show disorganization of the OS in Mfsd2a KO mice, and RPE appears swollen. *Scale bar,* 2 μm. The *middle panel* shows that villi Mfsd2a KO RPE appear thickened and interspersed with OS that are not formed properly relative to those seen in WT (*white arrow*). *Scale bar,* 2 μm. The *far right panel* is of the basal membrane of the RPE, where edema was also seen at the basal infoldings of Mfsd2a KO RPE but not in wild-type RPE (*yellow arrow*). *Scale bar,* 1 μm. *G,* immunolocalization of ezrin was performed on eye sections taken from P13 and 5-month-old mice. At age P13, Mfsd2a KO villi appears disorganized and collapsed onto itself at 5 months of age (*white arrows*). *Scale bar,* 20 μm. P13, $n = 3$ per genotype. *INL,* inner nuclear layer; *IS,* inner segment; *PR,* photoreceptor; *AM,* apical membrane; *BI,* basal infoldings.

TABLE 1
Gene list from ingenuity pathway analysis
Table shows the specific genes that were upregulated in MA plots shown in Fig. 6*D* and Fig. 9*C*.

Srebp1c	Srebp2	Microglia
Acsl4	*Aldoc*	*Abi1*
Aldoc	*Cyp51a1*	*Aif1*
Cyp51a1	*Dhcr7*	*Aif1l*
Dhcr7	*Fads2*	*Aldh1l1*
Fads1	*Fasn*	*Angptl4*
Fads2	*Idh1*	*C1qa*
Fasn	*Idi1*	*C1qb*
Gstm6	*Insig1*	*C1qc*
Hk2	*Ldlr*	*Ccl6*
Idh1	*Lss*	*Cd1d*
Idi1	*Mvd*	*Cd276*
Insig1	*Scd*	*Cd40*
Ldlr	*Srebf1*	*Cirbp*
Lss	*Srebf2*	*Coro1a*
Mvd	*Stard4*	*Ctss*
Scd		*Cx3cr1*
Scd2		*Cxcr4*
Srebf1		*Egf*
Stard4		*Egr1*
		Elavl1
		Fam107a
		Fasn
		Gart
		Gbp4
		Gbp6
		Gbp7
		Gjb2
		Gnb4
		Hk2
		Idi1
		Irf7
		Krt14
		Metap2
		Prdm1
		Psd2
		Rtp4
		S100a8
		S100a9
		Sema7a
		Slc1a3
		Spp1
		Srebf1
		Srebf2
		Stat1
		Tgfbr1
		Tyrobp
		Usp18
		Vcam1
		Xist

up-regulation of genes of the microglia/interferon pathway (Fig. 6*D* and Table 1).

To determine whether the pathological findings described above for Mfsd2a retina and RPE would affect visual function, electroretinography (ERG) was carried out in 4-month-old mice. Surprisingly, despite the disorganization of OS discs and shortened length of OS in eyes of Mfsd2a KO mice, ERG experiments indicated only small, non-significant reductions in visual function in Mfsd2a KO mice relative to wild-type mice (Fig. 7, *A* and *B*). Microglia activation as described above might serve as a protective mechanism in Mfsd2a KO mice to maintain eye function by clearing of subretinal debris. It is also possible that significant reductions in visual function in Mfsd2a KO were not detected because of a lack of sufficient sensitivity of our ERG analysis. Nonetheless, consistent with these functional studies, several key proteins involved in phototransduction and visual cycle were unchanged in Mfsd2a KO mice (Fig. 7, *C* and *D*).

Mfsd2a Expressed in the Retinal Vasculature Does Not Contribute to Eye DHA Accretion or Photoreceptor Survival—To determine whether the phenotypes observed in Mfsd2a KO mice were due to Mfsd2a deficiency in the retinal capillaries or RPE, we generated an endothelium-specific Mfsd2a KO model (LLTie2cre) by crossing mice with Mfsd2a floxed alleles (LL) with mice expressing Tie2Cre. As expected, immunolocalization of Mfsd2a in retinal flat mounts indicated that Mfsd2a was deleted in retinal capillaries (Fig. 8*A*). Western blot indicated that Mfsd2a was not deleted from RPE (Fig. 8*B*). The eyeballs of LLTie2cre mice were smaller than LL control mice, a finding similar to Mfsd2a KO mice, and related to the severe microcephaly exhibited by both mouse models (16, 20). Histological examination indicated that OS length relative to total photoreceptor length in 4-month-old LLTie2cre mice was comparable with LL control mice (Fig. 8, *C* and *D*). Consistent with normal OS length, lipidomics analysis of whole eyes by mass spectrometry indicated that the levels of DHA and AA in phospholipids of eyes of LLTie2Cre mice are comparable with LL control mice (Fig. 8*E*). Collectively, these findings indicate that Mfsd2a expressed in the RPE, but not the retinal vasculature, is essential for DHA accretion by the eye and photoreceptor development and survival.

Defective Rhodopsin Trafficking in Retinas of Mfsd2a KO Mice—The specific reduction in OS disc length at P13 in Mfsd2a KO eyes, an age at which the eyes are closed and active photoreceptor OS development takes place, together with the findings that Mfsd2a plays a quantitative role in LPC/DHA uptake into the eye across the RPE, raises the possibility that OS disc formation is defective. In line with this scenario, rhodopsin levels were found to be reduced as early as P13 before loss of ONL and remained low in adult mice (Fig. 9*A*). Immunolocalization of rhodopsin in P14 mice showed that rhodopsin was mislocalized to the ONL in Mfsd2a KO eyes, consistent with defects in rhodopsin trafficking (Fig. 9*B*). Mislocalization or accumulation of rhodopsin to the ONL has been associated with retinal degenerative diseases like retinitis pigmentosa (14).

Mfsd2a Deficiency Results in Up-regulation of Lipogenesis and Cholesterogenesis Pathways—One likely adaptive response in the eye to Mfsd2a deficiency is microglia migration to the subretinal space and their activation (Fig. 6). To further identify adaptations to Mfsd2a deficiency in the eye, transcriptome analysis was performed using microarrays from RNA isolated from the eye cups of P13 Mfsd2a KO and wild-type controls. Remarkably, the top two predicted pathways for up-regulated genes in Mfsd2a KO eyes were the lipogenic targets of the transcription factor Srebf1 (Srebp1) and cholesterogenic targets of the transcription factor Srebf2 (Srebp2) pathways (Fig. 9*C* and Table 1). These findings were validated by quantitative-PCR on selected genes from these two pathways (Fig. 9*D* and Table 2).

Discussion

The mechanism for the transport and accumulation of DHA in the retina has been a point of debate because specific transporters have not been identified. Here we demonstrated that Mfsd2a, a sodium-dependent LPC transporter, is highly expressed in the RPE and quantitatively important for DHA accretion in the retina via LPC/DHA transport. Moreover,

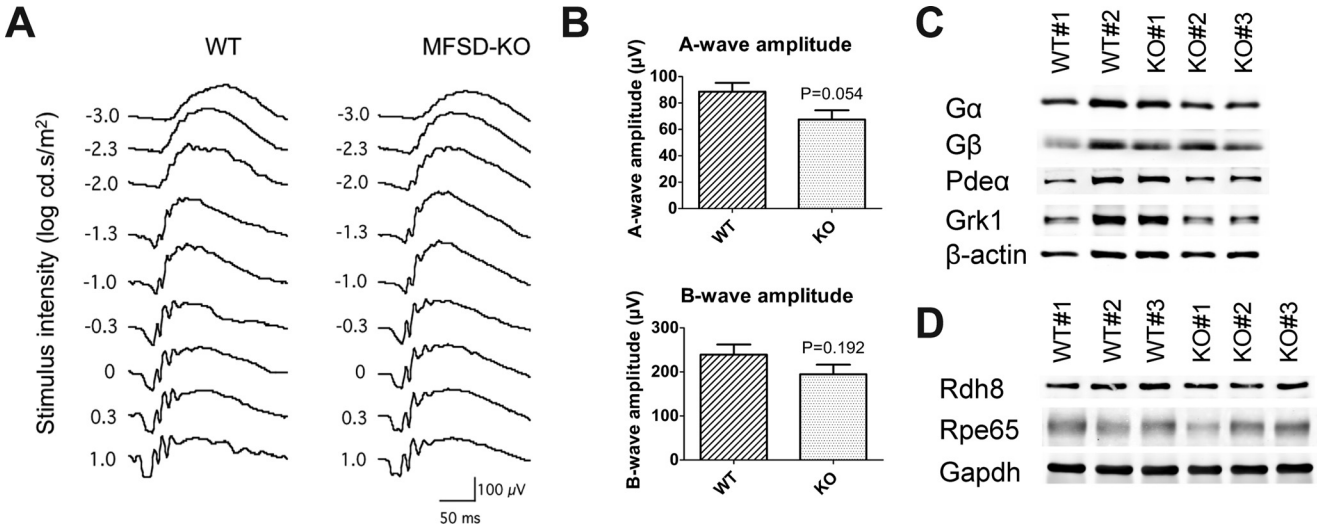

FIGURE 7. **Mfsd2a deficiency does not result in significant loss of visual function.** *A,* ERG waveforms taken at different stimulus intensities indicate that 4-month-old Mfsd2a KO mice have small but non-significant reductions in visual function relative to WT mice. *WT*, $n = 6$; *KO*, $n = 6$. *B,* A-wave and B-wave amplitude expressed as mean ± S.E. indicate that Mfsd2a KO mice have small but non-significant reductions in visual function. *WT*, $n = 6$; *KO*, $n = 6$. *C,* representative Western blot of some key proteins involved in phototransduction in whole eyes in 5-week-old mice. Expression levels are similar between wild-type and Mfsd2a KO mice. β-Actin served as a loading control. *WT*, $n = 2$; *KO*, $n = 3$. *D,* representative Western blot of two key proteins involved in retinol metabolism in the visual cycle in whole eyes in 8-week-old mice. Expression levels are similar between wild-type and Mfsd2a KO mice. GAPDH served as a loading control. *WT*, $n = 3$; *KO*, $n = 3$.

Mfsd2a KO mice have a unique form of a slow, progressive retina degeneration that primarily manifests early postnatally as a decrease in OS length.

Contrary to the widely held view that DHA is important for the maintenance of photoreceptor health (5), DHA deficiency in Mfsd2a KO mice (40% of wild-type) did not result in severe and rapid retinal degeneration nor significant visual impairment. Because we measured DHA in phospholipid pools of whole eye and not specifically in the retina, the 40% reduction in DHA might be an underestimate of the true amount in the retina of Mfsd2a KO mice. Nonetheless, DHA is present in Mfsd2a KO eyes implicating alternative mechanisms for DHA uptake into the eye (5). Another probable explanation for the significant amount of DHA in the eyes of Mfsd2a KO mice is that *de novo* synthesis of DHA is enhanced. In support of this possibility is the finding that Fads1 and Fads2 (31, 32), which are both Srebp1c targets and fatty acid desaturases critical for *de novo* synthesis of polyunsaturated fatty acids, were both significantly increased in eye cups of P13 KO mice (Fig. 9, *C* and *D*, and Table 1). Moreover, this increase in Fads1 and Fads2 might explain the minor increase in arachidonic acid and other long chain unsaturated fatty acids in Mfsd2a KO eyes. The early postnatal reduction in OS length without photoreceptor cell death was a striking feature of Mfsd2a KO retinas. The OS contains photoreceptor disc membranes that form through membrane biogenesis in the IS (11–13), occurring on a daily basis to balance photoreceptor disc turnover at the distal OS via phagocytosis by the RPE (10). It can be imagined that this high level of membrane biogenesis to build OS discs would apply unique metabolic demands on the retina. That the retina exhibits a high utilization for glucose, which is largely metabolized to lactate to maintain photoreceptor sodium transport and survival (33, 34), raises the possibility that *de novo* lipogenesis from glucose metabolism might not be sufficient to maintain OS membrane biogenesis. Consistent with this idea, the top two up-regulated gene pathways in the eye of Mfsd2a KO mice were Srebp1 and Srebp2, implicating up-regulation of *de novo* lipogenesis pathways as adaptations to maintaining OS membrane biogenesis. Thus, the transport of plasma-derived LPCs might provide an abundant source of membrane building blocks for photoreceptor OS disc development. Indeed, the liver is the primary source for plasma LPC where LPC levels circulate on albumin in human and rodent plasma at high concentrations similar to concentrations of unesterified fatty acids (18, 19, 35). The specific reduction in OS length in Mfsd2a KO mice might be analogous to the microcephaly observed in mice and humans with Mfsd2a loss-of-function mutations, in which LPCs are required for brain growth (16, 18, 19). Similar to the metabolic demands of the retina, neurons in the brain primarily consume glucose for production of ATP for the maintenance of cation pumps and membrane potential (36). The transport of LPC by Mfsd2a into the brain might spare glucose for this purpose and provide a readily available phospholipid source and conduit for DHA uptake for membrane biogenesis. It is important to note that generational dietary DHA deficiency in rodents resulted in eye DHA deficiency, but it has not been reported to result in photoreceptor degeneration (37), as described here for Mfsd2a KO mice. These findings suggest that the unique phenotype of reduced OS length in Mfsd2a KO retinas might be consequential to not only DHA deficiency but deficiency in phospholipid supply in the form of LPCs to the retina.

Another phenotype exhibited early in postnatal eye development in Mfsd2a KO mice was thickening of the RPE, collapsed apical villi, and edematous appearance of basal infoldings. One of the primary functions of the RPE is to mediate phagocytosis of OS segments. The RPE phagocytic activity is likely one of the highest for any known mammalian cell type, where one RPE cell would provide phagocytic support for ~40–60 photoreceptor cells (38). This interaction would result in a daily consumption

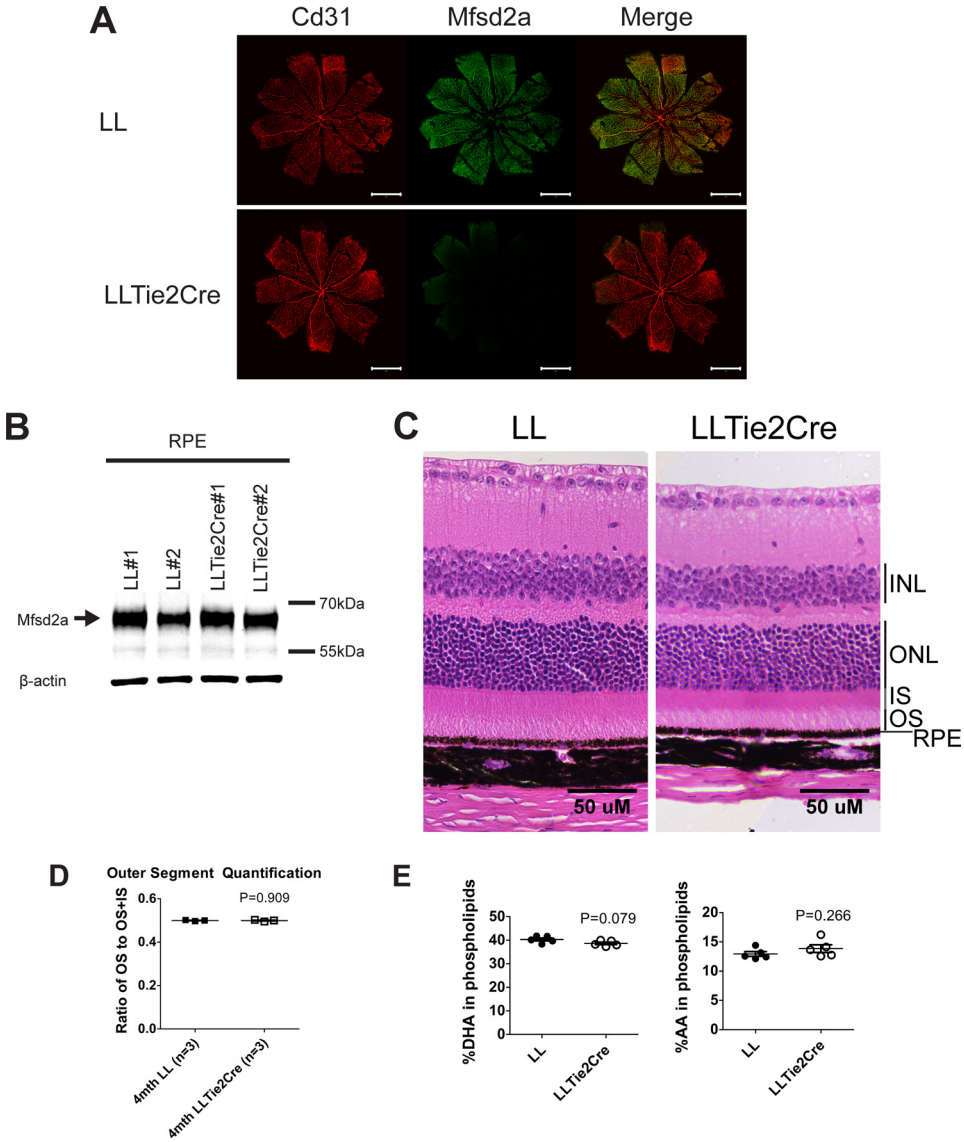

FIGURE 8. **Mfsd2a deficiency in retina vasculature does not contribute to eye DHA accretion or photoreceptor survival.** *A,* immunolocalization of Mfsd2a in capillaries of the developing eye. Retinal whole mounts were prepared from postnatal day 9 Mfsd2a floxed (*LL*) and LLTie2Cre mice and stained for the endothelial cell marker Cd31 and Mfsd2a. Mfsd2a is shown to be expressed only in capillaries of LL mice but absent in LLTie2Cre mice, consistent with deletion in retina vasculature. *Scale bar,* 1 mm. *LL*, $n = 2$; *LLTie2Cre*, $n = 2$. *B,* representative Western blot of Mfsd2a expression in RPE (eye cup without retina) of 6-week-old mice. As expected, Mfsd2a levels are similar between LL and LLTie2Cre RPE. β-Actin served as a loading control. *LL*, $n = 2$; *LLTie2Cre*, $n = 2$. *C,* H&E staining of eyes of 4-month-old mice was carried out to visualize the layers. Although eyes of LLTie2Cre mice appear slightly smaller, retina layers appear comparable with LL control. *LL*, $n = 3$; *LLTie2Cre*, $n = 4$. *Scale bar,* 50 μm. *D,* ratio of OS to OS + IS was quantified in eyes of 4-month-old mice. Ratios of OS length are comparable between eyes of LL and LLTie2Cre mice. *LL*, $n = 3$; *LLTie2Cre*, $n = 3$. *E,* comprehensive lipidomic analysis of whole eyes from 7-week-old mice. Total DHA and AA levels in eye phospholipids are expressed as mean ± S.E. of the percentage of the total level of phospholipids. *LL*, $n = 5$; *LLTie2Cre*, $n = 5$.

of ~3,200–4,800 OS discs (9, 38), with each disc having an average surface area of 2.86 μm^2 (9). This high level of phagocytosis, which results in endocytosis of large amounts of plasma membrane forming the phagosome membrane, would expect to impose a high demand for new membrane biogenesis. Interestingly, increasing phagocytosis in HEK293 cells resulted in enhanced biosynthesis of fatty acids and cholesterol at a level equivalent to the amount of plasma membrane lost during endocytosis, a process that was entirely controlled by activation of Srebp1 and Srebp2 (39). Similarly, Srebp1 and Srebp2 gene targets were the top up-regulated pathways in the eyes of Mfsd2a KO mice, suggesting a compensatory mechanism to maintain membrane biogenesis in the absence of Mfsd2a. It is therefore plausible that LPCs transported by Mfsd2a might also contribute to the phospholipid pool for apical membrane regeneration in RPE cells. The cell types that might exhibit up-regulation of *de novo* lipogenesis in eyes of Mfsd2a KO mice remain to be determined.

We found that genetic deletion of Mfsd2a in vascular endothelium did not affect retina morphology or DHA levels in the eye, consistent with the RPE as the primary site of Mfsd2a expression. In addition, the BRB was found to be intact in Mfsd2a KO mice. Surprisingly, the BBB were not leaky in our Mfsd2a KO mouse model, which is inconsistent with a recent report concluding that Mfsd2a is critical for BBB formation and function (25). We do not have an explanation for this discrep-

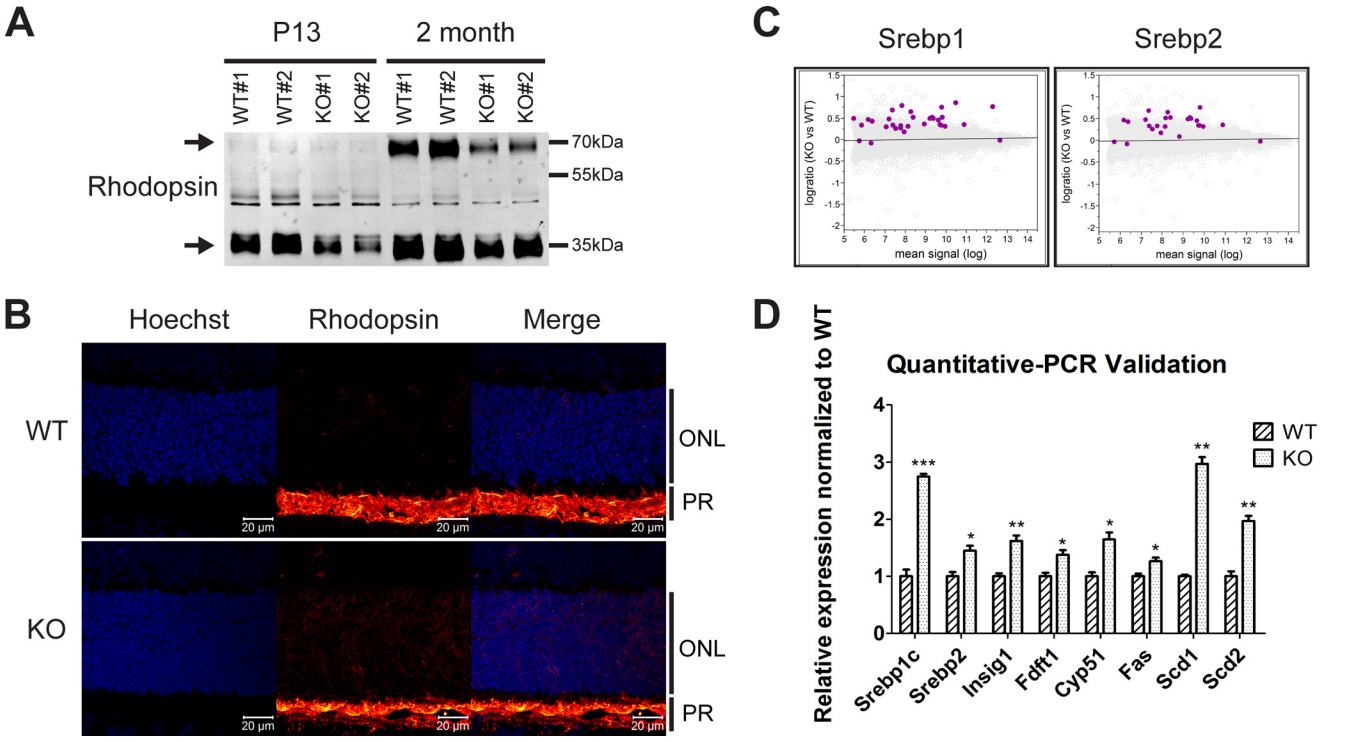

FIGURE 9. **Mfsd2a deficiency results in reduced rhodopsin levels and mislocalization and up-regulation of lipogenesis pathways.** *A,* representative Western blot of rhodopsin expression in whole eyes in P13 and 2-month-old mice. Reduced rhodopsin expression is seen in Mfsd2a KO mice as early as P13. *Black arrows* indicate monomeric and dimeric rhodopsin. P13, $n = 2$ per genotype; 2-month-old mice, $n = 4$ per genotype. *B,* immunolocalization of rhodopsin was performed on eye sections from P14 mice. Rhodopsin, which normally resides in the OS, as seen in WT, was found to be mislocalized to the ONL layer in Mfsd2a KO retina. *Scale bar,* 20 μm. *WT*, $n = 5$; *KO*, $n = 5$. *C,* gene microarray analysis from P13 eye cups of WT and Mfsd2a KO mice. An MA plot, which is used to visualize intensity-dependent ratio of raw gene microarray data, indicated that the top predicted up-regulated genes in Mfsd2a KO eyes are the lipogenic and cholesterogenic Srebp1 and Srebp2 pathways, respectively. *Purple dots* on each *graph* represent individual Srebp1 and Srebp2 targets over the background of expressed genes. *D,* quantitative-PCR was carried out on selected panel to validate gene array findings. *WT*, $n = 4$; *KO*, $n = 4$. ***, $p < 0.0001$; **, $p < 0.01$; *, $p < 0.05$. PR, photoreceptor.

TABLE 2
Primers for quantitative-PCR

Gene	Forward (5′ to 3′)	Reverse (5′ to 3′)
Srebp1c	ATCGGCGCGGAAGCTGTCGGGGTAGCGTC	ACTGTCTTGGTTGTTGATGAGCTGGAGCAT
Srebp2	GCAGCAACGGGACCATTCT	CCCCATGACTAAGTCCTTCAACT
Insig1	TGCAGATCCAGCGGAATGT	CCAGGCGGAGGAGAAGATG
FdFt1	ATGGAGTTCGTCAAGTGTCTAGG	CGTGCCGTATGTCCCCATC
Cyp51	GACAGGAGGCAACTTGCTTTC	GTGGACTTTTCGCTCCAGC
Fas	CCAGGAGAGACTGTCACAAGG	ACTGGGATCCTCTGAACACCT
Scd1	TTCTTGCGATACACTCTGGTGC	CGGGATTGAATGTTCTTGTCGT
Scd2	GCATTTGGGAGCCTTGTACG	AGCCGTGCCTTGTATGTTCTG

ancy, but the possibility remains that BBB leakage is mouse strain-specific in that a modifier gene(s) could compensate for the absence of Mfsd2a, which would indicate a minor role at best of Mfsd2a in regulating BBB integrity. Moreover, humans with loss-of-function mutations in Mfsd2a did not present with evidence of BBB disruption (18, 19).

The location of Mfsd2a at the RPE raises the possibility that Mfsd2a transport function could be exploited for delivering small molecules to the RPE and retina. One approach might be to conjugate small molecule therapeutics to LPC scaffolds for delivery to the back of the eye to treat eye diseases such as adult-onset macular degeneration, the most common cause for blindness in developed countries and affecting those above the age of 50 (40, 41). To date, the treatment of adult-onset macular degeneration is limited and largely managed through the invasive approach of ocular injection of anti-angiogenic therapeutics (41). Exploring the transport potential of Mfsd2a for drug delivery warrants careful attention. In summary, the findings here support the Mfsd2a is a LPC transporter in the eye and a major route for DHA accretion in the eye. These findings present an opportunity to understand the mechanism by which LPCs contribute to membrane biogenesis of photoreceptor outer segments and RPE function, processes critical for visual function.

Author Contributions—D. L. S. and B. H. W. designed the research. B. H. W. performed the majority of experiments. J. P. C. performed blood-brain barrier permeability experiments. A. C.-G. and J. C. F. performed lipidomic mass spectrometry analysis. R. W. P. assisted with electron microscopy studies. D. L. A. G. assisted with transport assays. S. W. Y., V. A. B., and C. D. L. performed ERG analysis. L. N. N. assisted with lipidomic analysis. M. R. W. contributed new analytic tools for mass spectrometry. S. G. performed pathway analysis for gene array data. B. H. W. and D. L. S. analyzed all data and wrote the paper.

Acknowledgments—We acknowledge the use of the facilities and the scientific and technical assistance or the Advanced Bio-imaging Core at The Academia, Singapore Health Services.

References

1. SanGiovanni, J. P., and Chew, E. Y. (2005) The role of ω-3 long-chain polyunsaturated fatty acids in health and disease of the retina. *Prog. Retin. Eye Res.* **24,** 87–138
2. Kidd, P. M. (2007) ω-3 DHA and EPA for cognition, behavior, and mood: clinical findings and structural-functional synergies with cell membrane phospholipids. *Altern. Med. Rev.* **12,** 207–227
3. Fliesler, S. J., and Anderson, R. E. (1983) Chemistry and metabolism of lipids in the vertebrate retina. *Prog. Lipid Res.* **22,** 79–131
4. Cunha-Vaz, J. (1979) The blood-ocular barriers. *Surv. Ophthalmol.* **23,** 279–296
5. Bazan, N. G. (2006) Cell survival matters: docosahexaenoic acid signaling, neuroprotection and photoreceptors. *Trends Neurosci.* **29,** 263–271
6. Young, R. W. (1976) Visual cells and the concept of renewal. *Invest. Ophthalmol. Vis. Sci.* **15,** 700–725
7. Steinberg, R. H. (1985) Interactions between the retinal pigment epithelium and the neural retina. *Doc. Ophthalmol.* **60,** 327–346
8. Bosch, E., Horwitz, J., and Bok, D. (1993) Phagocytosis of outer segments by retinal pigment epithelium: phagosome-lysosome interaction. *J. Histochem Cytochem.* **41,** 253–263
9. Liang, Y., Fotiadis, D., Maeda, T., Maeda, A., Modzelewska, A., Filipek, S., Saperstein, D. A., Engel, A., and Palczewski, K. (2004) Rhodopsin signaling and organization in heterozygote rhodopsin knockout mice. *J. Biol. Chem.* **279,** 48189–48196
10. Young, R. W. (1967) The renewal of photoreceptor cell outer segments. *J. Cell Biol.* **33,** 61–72
11. Burgoyne, T., Meschede, I. P., Burden, J. J., Bailly, M., Seabra, M. C., and Futter, C. E. (2015) Rod disc renewal occurs by evagination of the ciliary plasma membrane that makes cadherin-based contacts with the inner segment. *Proc. Natl. Acad. Sci. U.S.A.* **112,** 15922–15927
12. Volland, S., Hughes, L. C., Kong, C., Burgess, B. L., Linberg, K. A., Luna, G., Zhou, Z. H., Fisher, S. K., and Williams, D. S. (2015) Three-dimensional organization of nascent rod outer segment disk membranes. *Proc. Natl. Acad. Sci. U.S.A.* **112,** 14870–14875
13. Ding, J. D., Salinas, R. Y., and Arshavsky, V. Y. (2015) Discs of mammalian rod photoreceptors form through the membrane evagination mechanism. *J. Cell Biol.* **211,** 495–502
14. Price, B. A., Sandoval, I. M., Chan, F., Simons, D. L., Wu, S. M., Wensel, T. G., and Wilson, J. H. (2011) Mislocalization and degradation of human P23H-rhodopsin-GFP in a knockin mouse model of retinitis pigmentosa. *Invest. Ophthalmol. Vis. Sci.* **52,** 9728–9736
15. Ferrari, S., Di Iorio, E., Barbaro, V., Ponzin, D., Sorrentino, F. S., and Parmeggiani, F. (2011) Retinitis pigmentosa: genes and disease mechanisms. *Curr. Genomics* **12,** 238–249
16. Nguyen, L. N., Ma, D., Shui, G., Wong, P., Cazenave-Gassiot, A., Zhang, X., Wenk, M. R., Goh, E. L., and Silver, D. L. (2014) Mfsd2a is a transporter for the essential ω-3 fatty acid docosahexaenoic acid. *Nature* **509,** 503–506
17. Ethayathulla, A. S., Yousef, M. S., Amin, A., Leblanc, G., Kaback, H. R., and Guan, L. (2014) Structure-based mechanism for Na^+/melibiose symport by MelB. *Nat. Commun.* **5,** 3009
18. Alakbarzade, V., Hameed, A., Quek, D. Q., Chioza, B. A., Baple, E. L., Cazenave-Gassiot, A., Nguyen, L. N., Wenk, M. R., Ahmad, A. Q., Sreekantan-Nair, A., Weedon, M. N., Rich, P., Patton, M. A., Warner, T. T., Silver, D. L., *et al.* (2015) A partially inactivating mutation in the sodium-dependent lysophosphatidylcholine transporter MFSD2A causes a non-lethal microcephaly syndrome. *Nat. Genet.* **47,** 814–817
19. Guemez-Gamboa, A., Nguyen, L. N., Yang, H., Zaki, M. S., Kara, M., Ben-Omran, T., Akizu, N., Rosti, R. O., Rosti, B., Scott, E., Schroth, J., Copeland, B., Vaux, K. K., Cazenave-Gassiot, A., Quek, D. Q., *et al.* (2015) Inactivating mutations in MFSD2A, required for ω-3 fatty acid transport in brain, cause a lethal microcephaly syndrome. *Nat. Genet.* **47,** 809–813
20. Berger, J. H., Charron, M. J., and Silver, D. L. (2012) Major facilitator superfamily domain-containing protein 2a (MFSD2A) has roles in body growth, motor function, and lipid metabolism. *PLoS One* **7,** e50629
21. Robinson, R., Ho, C. E., Tan, Q. S., Luu, C. D., Moe, K. T., Cheung, C. Y., Wong, T. Y., and Barathi, V. A. (2011) Fluvastatin downregulates VEGF-A expression in TNF-α-induced retinal vessel tortuosity. *Invest. Ophthalmol. Vis. Sci.* **52,** 7423–7431
22. Tual-Chalot, S., Allinson, K. R., Fruttiger, M., and Arthur, H. M. (2013) Whole mount immunofluorescent staining of the neonatal mouse retina to investigate angiogenesis *in vivo*. *J. Vis. Exp.* **77,** e50546
23. Wang, Y., Rattner, A., Zhou, Y., Williams, J., Smallwood, P. M., and Nathans, J. (2012) Norrin/Frizzled4 signaling in retinal vascular development and blood brain barrier plasticity. *Cell* **151,** 1332–1344
24. Byrne, L. C., Lin, Y. J., Lee, T., Schaffer, D. V., and Flannery, J. G. (2015) The expression pattern of systemically injected AAV9 in the developing mouse retina is determined by age. *Mol. Ther.* **23,** 290–296
25. Ben-Zvi, A., Lacoste, B., Kur, E., Andreone, B. J., Mayshar, Y., Yan, H., and Gu, C. (2014) Mfsd2a is critical for the formation and function of the blood-brain barrier. *Nature* **509,** 507–511
26. Armulik, A., Genové, G., Mäe, M., Nisancioglu, M. H., Wallgard, E., Niaudet, C., He, L., Norlin, J., Lindblom, P., Strittmatter, K., Johansson, B. R., and Betsholtz, C. (2010) Pericytes regulate the blood-brain barrier. *Nature* **468,** 557–561
27. Daneman, R., Zhou, L., Kebede, A. A., and Barres, B. A. (2010) Pericytes are required for blood-brain barrier integrity during embryogenesis. *Nature* **468,** 562–566
28. Winkler, E. A., Bell, R. D., and Zlokovic, B. V. (2011) Central nervous system pericytes in health and disease. *Nat. Neurosci.* **14,** 1398–1405
29. Simopoulos, A. P. (2008) The importance of the ω-6/ω-3 fatty acid ratio in cardiovascular disease and other chronic diseases. *Exp. Biol. Med.* **233,** 674–688
30. Langmann, T. (2007) Microglia activation in retinal degeneration. *J. Leukocyte Biol.* **81,** 1345–1351
31. Cho, H. P., Nakamura, M., and Clarke, S. D. (1999) Cloning, expression, and fatty acid regulation of the human Δ-5 desaturase. *J. Biol. Chem.* **274,** 37335–37339
32. Cho, H. P., Nakamura, M. T., and Clarke, S. D. (1999) Cloning, expression, and nutritional regulation of the mammalian Δ-6 desaturase. *J. Biol. Chem.* **274,** 471–477
33. Chertov, A. O., Holzhausen, L., Kuok, I. T., Couron, D., Parker, E., Linton, J. D., Sadilek, M., Sweet, I. R., and Hurley, J. B. (2011) Roles of glucose in photoreceptor survival. *J. Biol. Chem.* **286,** 34700–34711
34. Lindsay, K. J., Du, J., Sloat, S. R., Contreras, L., Linton, J. D., Turner, S. J., Sadilek, M., Satrústegui, J., and Hurley, J. B. (2014) Pyruvate kinase and aspartate-glutamate carrier distributions reveal key metabolic links between neurons and glia in retina. *Proc. Natl. Acad. Sci. U.S.A.* **111,** 15579–15584
35. Croset, M., Brossard, N., Polette, A., and Lagarde, M. (2000) Characterization of plasma unsaturated lysophosphatidylcholines in human and rat. *Biochem. J.* **345,** 61–67
36. Harris, J. J., Jolivet, R., and Attwell, D. (2012) Synaptic energy use and supply. *Neuron* **75,** 762–777
37. Weisinger, H. S., Armitage, J. A., Jeffrey, B. G., Mitchell, D. C., Moriguchi, T., Sinclair, A. J., Weisinger, R. S., and Salem, N., Jr. (2002) Retinal sensitivity loss in third-generation *n*-3 PUFA-deficient rats. *Lipids* **37,** 759–765
38. Mustafi, D., Kevany, B. M., Genoud, C., Bai, X., and Palczewski, K. (2013) Photoreceptor phagocytosis is mediated by phosphoinositide signaling. *FASEB J.* **27,** 4585–4595
39. Castoreno, A. B., Wang, Y., Stockinger, W., Jarzylo, L. A., Du, H., Pagnon, J. C., Shieh, E. C., and Nohturfft, A. (2005) Transcriptional regulation of phagocytosis-induced membrane biogenesis by sterol regulatory element binding proteins. *Proc. Natl. Acad. Sci. U.S.A.* **102,** 13129–13134
40. Ambati, J., Ambati, B. K., Yoo, S. H., Ianchulev, S., and Adamis, A. P. (2003) Age-related macular degeneration: etiology, pathogenesis, and therapeutic strategies. *Surv. Ophthalmol.* **48,** 257–293
41. Amadio, M., Govoni, S., and Pascale, A. (2016) Targeting VEGF in eye neovascularization: What's new? A comprehensive review on current therapies and oligonucleotide-based interventions under development. *Pharmacol. Res.* **103,** 253–269